Evaluation of Nitrogen Nuclear Hyperfine and Quadrupole Coupling Parameters for the Proximal Imidazole in Myoglobin–Azide, –Cyanide, and –Mercaptoethanol Complexes by Electron Spin Echo Envelope Modulation Spectroscopy†

Richard S. Magliozzo*,‡ and Jack Peisach‡,§

Department of Molecular Pharmacology and Department of Physiology and Biophysics, Albert Einstein College of Medicine of Yeshiva University, Bronx, New York 10461

Received March 15, 1993; Revised Manuscript Received June 14, 1993

ABSTRACT: Electron spin echo envelope modulation (ESEEM) spectroscopy and computer simulation of spectra has been used to evaluate the nitrogen nuclear hyperfine and quadrupole coupling parameters for the proximal imidazole nitrogen directly coordinated to iron in three low-spin heme complexes, myoglobin–azide, –cyanide, and –mercaptoethanol (MbN_3, MbCN, and MbRS). The variability in the weak electron–nuclear coupling parameters reveals the electronic flexibility within the heme group that depends on properties of the exogenous ligands. For example, the isotropic component of the nitrogen nuclear hyperfine coupling ranges from 4.4 MHz for MbN_3 to 2.2 MHz for both MbCN and MbRS. The weaker coupling in MbCN and MbRS is taken as evidence for delocalization of unpaired electron spin from iron into the exogenous anionic ligands. The value of e^2Qq, the nuclear quadrupole coupling constant for the axial imidazole nitrogen in MbCN and MbRS, was 2.5 MHz but was significantly larger, 3.2 MHz, in MbN_3. This large value is considered evidence for a weakened σ bond between the proximal imidazole and ferric iron in this form, and for a feature contributing to the origin of the high spin–low spin equilibrium exhibited by MbN_3 [Beetlestone, J., & George, P. (1964) *Biochemistry 5*, 707–714]. The ESEEM results have allowed a correlation to be made between the orientation of the g tensor axes, the orientation of the p–π orbital of the proximal imidazole nitrogen, and σ- and π-bonding features of the axial ligands. Furthermore, the proximal imidazole is suggested to act as a π-acceptor in low-spin heme complexes in order to support strong σ electron donation from the lone pair orbital to iron. An evaluation of the nitrogen nuclear hyperfine coupling parameters for the porphyrin pyrrole sites in MbRS reveals a large inequivalence in isotropic components consistent with an orientation of rhombic axes (and g tensor axes) that eclipses the $Fe–N_{pyrrole}$ vector directions.

The application of magnetic resonance spectroscopic techniques to the study of heme proteins has been aimed at issues concerning both structural and electronic features of the prosthetic group. The approaches for a variety of heme complexes include single-crystal EPR and ENDOR[1] studies (Hori, 1971; Helcké et al., 1968; Peisach et al., 1971; Scholes et al., 1982), extensive solution NMR experiments [see, for example, Satterlee (1986), Emerson and La Mar (1990a,b), and Wu et al. (1991)], and studies of models for which known structural parameters can be correlated with spectroscopic features (Walker et al., 1986; Soltis et al., 1988; Walker & Simonis, 1991; Safo et al., 1991, 1992). A central issue in this research has remained the advancement of an understanding of how proximal and distal effects at the prosthetic group modulate the functions of heme proteins and enzymes. In myoglobin, and in peroxidases such as cytochrome *c* peroxidase, the heme has an endogenous axial imidazole ligand supplied by a histidine residue and a sixth ligand site where exchangeable ligands, such as O_2, bind in the globins or substrates such as H_2O_2 react in the peroxidases (Takano, 1977; Philips, 1980; Poulos et al., 1980; Finzel et al., 1984). The chemistry of the heme that governs properties such as ligand affinity, substrate binding, or midpoint reduction potentials can be better understood when electronic parameters related to the features of axial as well as equatorial bonds in the prosthetic group have been evaluated.

NMR studies of the paramagnetic forms of heme proteins provide structural and electronic information through the observation of hyperfine-shifted resonances (Satterlee, 1986). In general, the NMR spectroscopy of ferric heme proteins is limited to high-spin forms and to the low-spin cyanide form. A recent report has demonstrated that the g tensor principal axis system for MbCN can be assigned in the molecular frame when a large number of hyperfine-shifted resonances are characterized, including those from residues near the heme but not covalently bound to the prosthetic group (Emerson & La Mar, 1990). This approach cannot be applied to other low-spin Mb complexes, such as MbN_3 and MbOH, because these exhibit a high spin–low spin equilibrium at room temperature (Beetlestone & George, 1964; Iizuka & Kotani, 1969; Desbois et al., 1979; Vickery et al., 1975) that interferes with a rigorous interpretation of chemical shift information (Iizuka & Morishima, 1974). For this reason, an analysis of trends in electronic features of the iron–nitrogen ligand bonds that would be provided through study of the hyperfine-shifted resonances for a group of low spin Mb complexes cannot be achieved.

† This work was supported by Grants GM-40168 and RR-02583 from the National Institutes of Health.

‡ Department of Molecular Pharmacology.

§ Department of Physiology and Biophysics.

[1] Abbreviations: ESEEM, electron spin echo envelope modulation; ENDOR, electron–nuclear double resonance; P, porphyrin; PPIX, protoporphyrin IX; TPP, tetraphenylporphyrin; Mb, myoglobin; metMb, metmyoglobin; MbCN, cyanometmyoglobin; MbN_3, azidometmyoglobin; MbRS, metmyoglobin–mercaptoethanol; RS, β-mercaptoethanol; nqi, nuclear quadrupole interaction; nqr, nuclear quadrupole resonance; imid, imidazole.

0006-2960/93/0432-8446$04.00/0

EPR studies of low-spin ferric heme proteins are limited due to the general lack of ligand hyperfine information though structural information can sometimes be provided through an analysis of crystal field parameters known as the tetragonal and rhombic splittings, calculated from the g values observed experimentally (Griffith, 1957; Blumberg & Peisach, 1971; Bohan, 1977; Taylor, 1977). This approach is also limited, however, in that it will not separately treat the effects of the axial (fifth and sixth) iron ligands. For heme proteins such as the b-type cytochromes, in which the heme has two axial imidazole ligands (Mathews et al., 1979), the orientation of the imidazole planes can be predicted from EPR spectral parameters on the basis of analogies to the spectra of well-characterized model complexes (Walker et al., 1986).

Electron spin echo envelope modulation (ESEEM) spectroscopy is a pulsed EPR technique that can supply the electronic parameters, such as electron–nuclear coupling constants, that are too weak to be resolved by conventional continuous wave EPR (Mims & Peisach, 1989). ESEEM at X-band is well suited to study low-spin heme because the magnitude of hyperfine interactions for both axial and pyrrole nitrogen ligands in many complexes falls within a range amenable to the technique. Furthermore, computer simulation of spectra based on a spin Hamiltonian that incorporates nitrogen nuclear quadrupole interactions in addition to anisotropic nitrogen nuclear hyperfine interactions can provide parameters associated with the σ bond between the proximal imidazole nitrogen and the iron atom, as well as parameters related to the unpaired spin interactions throughout the metal–ligand system (Cornelius et al., 1990; Magliozzo & Peisach, 1992).

A recent ESEEM spectroscopic study (Magliozzo & Peisach, 1992) reported the nuclear quadrupole and hyperfine interaction parameters for the directly bound nitrogen of the proximal imidazole in myoglobin hydroxide and in related model complexes containing nitrogen plus oxygen axial ligands. It was demonstrated that the principal axis system of the nuclear quadrupole interaction tensor for the proximal imidazole nitrogen could be used to assign the direction of g_z, the largest principal axis component of the rhombic g tensor. The assignment of g_z to the direction of the heme normal in MbOH is in accord with single-crystal EPR (Gibson et al., 1958) and solution MCD analyses (Eglinton et al., 1983).[2]

In the present report, a range of hyperfine and nuclear quadrupole coupling interactions are reported for the proximal imidazole nitrogen in low spin Mb complexes containing azide, cyanide or thiolate (β-mercaptoethanol) ligands. Changes in σ- and π-bonding features either are directly evaluated or are inferred from the coupling parameters obtained by simulation of spectra. Furthermore, the parameters have been correlated with known orientations of the g tensor axis systems and allow predictions about these axes to be made for an example in which the orientation is not known. The results reveal the electronic flexibility within the heme structure that depends on the properties of ligands bound on the distal side. Though these results are not directly informative about myoglobin in its normal physiological state, they are relevant to the understanding of the relationship between structure and electronic features for low-spin ferric heme proteins in general.

[2] At the time this technique was applied to the analysis of MbOH, we were not aware of the single-crystal EPR study of this low-spin form (Gibson et al., 1958).

MATERIALS AND METHODS

Horse metMb (Sigma) was used without further purification. It was converted to the apoprotein (Teale, 1959) and was reconstituted with [^{15}N]heme (generously provided by Dr. Kevin Smith) according to a published procedure (Ascoli et al., 1981) with minor modifications. The reconstituted [^{15}N]heme metMb was concentrated to approximately 3 mM by ultrafiltration. In the interest of sample conservation, various low-spin forms of this protein were prepared from a starting sample of [^{15}N]heme MbOH used in an earlier study (Magliozzo & Peisach, 1992). Thus, the azide complex was prepared by adding 30 μL of 0.3 M $Na^{15}N_3$ (Isotec, Inc.), buffered to pH 7.0 with KH_2PO_4, to 150 μL of 3 mM [^{15}N]-heme MbOH. The continuous wave EPR spectrum of this sample (77 K) indicated complete conversion to MbN_3 (g = 2.78, 2.21, 1.73) (Helcké et al., 1968). The [^{15}N]heme MbN_3 sample was converted to [^{15}N]heme MbCN (reported g = 3.45, 1.89, 0.93; Peisach et al., 1971) by ultrafiltration to exchange the buffer to 50 mM KCN in 0.1 M potassium phosphate, pH 7.6. MbRS (g = 2.41, 2.24, 1.93) was prepared from Mb in phosphate buffer by addition of β-mercaptoethanol to a final concentration of $\approx$1%. The g values observed for MbRS are nearly equal to those reported by Chevion et al. (1977).

Electron spin echo envelopes were recorded at liquid helium temperatures (either 4 or 1.8 K) using a pulsed EPR spectrometer and methodology previously described (McCracken et al., 1987). The ESEEM spectra presented here are the Fourier transforms of spin echo decay envelopes recorded in three-pulse (stimulated echo) experiments (Peisach et al., 1979; Mims & Peisach, 1989). The value of τ was chosen such that the modulations due to hydrogen nuclei were suppressed (Peisach et al., 1979).

The evaluation of coupling parameters for the $S = {}^1/_2$, $I = 1$ electron–nuclear spin system, in which the largest anisotropy is in the g tensor, was achieved by simulation of the ESEEM spectra at two or more well-separated magnetic field settings within the EPR absorption. The computer programs and the approach used here were described previously for complexes in which the nitrogen nuclear hyperfine couplings were large compared to the nitrogen nuclear Zeeman interaction (Magliozzo & Peisach, 1992). For two of the three cases reported here (MbRS and MbCN) the weaker electron–nuclear coupling is of a magnitude that results in "exact cancellation" (Mims & Peisach, 1978; Flanagan & Singel, 1987) of nitrogen nuclear Zeeman and nuclear hyperfine interactions. The ESEEM spectrum then contains four components, three of which correspond closely to the zero-field nqr frequencies ν_+, ν_-, and ν_0 (Lucken, 1969), which depend on the nqi parameters e^2Qq (nitrogen nuclear quadrupole coupling constant) and η (quadrupole interaction asymmetry parameter) for a chosen value of the hyperfine coupling (Mims & Peisach, 1989; Jiang et al., 1990). The value of the hyperfine coupling ($a_{iso} = {}^1/_3[A_z + A_y + A_x]$, all terms being negative) is readily estimated by simulation of the highest frequency component, which arises from a $\Delta m_I = 2$ transition (Mims & Peisach, 1989). The evaluation of the nqi parameters, which is straightforward for the exact cancellation case, can be more difficult and may invoke larger errors for cases where the nitrogen nuclear hyperfine coupling is greater than $\sim$2 MHz (MbN_3). The simulation of spectra for [^{15}N]heme $Mb^{15}N_3$ was accomplished essentially as in a previously described approach (Magliozzo & Peisach, 1992) in which the magnitude and the anisotropy of the nitrogen nuclear hyperfine coupling was estimated from the position

of the highest frequency lines in spectra recorded near the extremes of the EPR absorption. The placement into the appropriate frequency range of the entire set of components in a simulation is thus approximated. Since the components exhibit different dependencies on the nitrogen nuclear hyperfine and nuclear quadrupole interaction parameters, the values of e^2Qq and η are also evaluated by simulation of spectra at more than one experimental field setting.

The g values for the low-spin complexes are assigned such that $g_z > g_y > g_x$. The Euler rotation angles giving the relationship of the principal axis elements of the nitrogen nuclear hyperfine and the nqi tensors to the g tensor elements are also evaluated in the process of simulation. The simulations generally show a strong dependence on the rotation angle, β, for the nqi axis system; this is the angle between the largest component, Q_{zz}, of the electric field gradient tensor describing the nuclear quadrupole interaction and the g tensor principal axis, g_z. For the *imino* nitrogen of the proximal imidazole, Q_{zz} is expected to lie along the nitrogen lone pair donor orbital (Ashby et al., 1978). This lobe of the sp^2 hybrid orbital forms a σ bond to the iron atom and thus also defines the heme normal (the molecular z axis). The orientation of the g tensor principal axes for MbN_3 is assumed to be as reported in single-crystal EPR (Helcké et al., 1968) and Mossbauer studies (Harami, 1979; Rhynard et al., 1979).[3] The g_z axis lies near the heme normal (Helcké et al., 1968; Hori, 1971), and g_y lies between an $Fe-N_{pyrrole}$ vector and a meso carbon position (Helcké, 1968; Harami, 1979). For MbCN, the g tensor is taken to be as reported by Peisach et al. (1971) and Shulman et al. (1971). These reports are in agreement with the rhombic axes reported from a Mossbauer analysis of MbCN (Rhynard et al., 1979). No single-crystal EPR data are available for MbRS.

The Euler angle, β, for the rotation of A_z (the smallest component of the nitrogen nuclear hyperfine interaction) onto the g_z axis is small for the simulations presented. This is the expected result for the directly coordinated proximal imidazole nitrogen when g_z occurs along the heme normal and the value of a_{iso} is negative (see below). The g_y and g_x axis directions and the directions of A_y and A_x, as well as the directions of Q_{yy} and Q_{xx}, those nqi axes perpendicular to the heme normal (i.e., perpendicular to Q_{zz}), are collinear (or nearly so) in all simulations; i.e., the Euler angles α and γ are zero or close to zero for the rotation of these hyperfine and quadrupole principal axes into the g tensor frame. Small values (20°) for the angles α and γ led to small shifts in the frequency of certain components, but no significant improvement in simulations was achieved by introduction of large angles. Furthermore, the location of the Q_{yy} and Q_{xx} axis directions in the coordinated imidazole nitrogen can only be assumed, and therefore no correlation would be unambiguously made between the values of these angles and structural parameters such as the "twist" and "roll" of the imidazole plane (Flanagan & Singel, 1987) even for a case in which the location of the g_y and g_x axes is known in the molecular frame.

In all cases, the fitting of simulations to spectra by eye is completed by trial and error. In general, the errors associated with the various coupling parameters are not greater than 10% but may be larger for the Euler rotation angles as well as for the value of η.

[3] There is some disagreement about the location of the in-plane axis directions (g_y and g_x) in the EPR reports for MbN_3 (Helcké et al., 1968; Hori, 1971), though a single-crystal Mossbauer study (Harami, 1979) and one of the single-crystal EPR studies (Helcké et al., 1968) agree on the placement of the g_y axis (see Discussion).

Fourier transforms of both ESEEM data and simulations are used for fitting, which introduces additional parameters into the procedure, some of which may affect the apparent intensities. For cases in which exact cancellation occurs, the lines in the ESEEM spectra are very sharp because of deep modulations that decay only slowly in stimulated echo envelopes (Mims & Peisach, 1989). The line widths in ESEEM spectra for species having electron–nuclear coupling away from exact cancellation are in general larger. Nevertheless, the same or very similar parameters were used in the decay functions applied in all simulations presented here.

RESULTS

The ESEEM techniques applied here allow the calculation of parameters related to the energies of nitrogen nuclear spin states for the axial and equatorial ligands. The energies depend on the strengths of three interactions including the nuclear Zeeman, hyperfine, and quadrupole couplings. The relevant hyperfine coupling parameters are presented as a_{iso} (the isotropic hyperfine term) and A_z, A_y, and A_x, which are the terms describing the coupling interaction along axes near the respective g tensor axes. The nuclear quadrupole interaction is described by a coupling constant e^2Qq and an asymmetry parameter η, both of which depend on electronic features of the ^{14}N valence shell and are related to the behavior of the lone pair of electrons in the nitrogen–iron σ bond.

Nuclear Hyperfine and Quadrupole Couplings for the Proximal Imidazole Nitrogen. The metMb used to prepare the azide and cyanide complexes for ESEEM spectroscopy contained [^{15}N]heme. This isotopic substitution simplified analysis of the axial ligand contributions in the ESEEM spectra because contributions from the [^{15}N]pyrrole sites do not appear in the data (Magliozzo & Peisach, 1992). No ESEEM spectra of model complexes are presented here as the relevant series of mixed-ligand Fe(III) porphyrins is difficult to generate in solution due to large differences in affinities for ligands such as cyanide and imidazole. Furthermore, the axial imidazole would not necessarily adopt an invariant position with respect to the porphyrin plane in a series of models in solution. For these reasons, the protein complexes, having constant equatorial ligands and a fixed proximal imidazole, provide the samples that best enable electronic changes induced by the exogenous ligands to be monitored.

Figure 1 shows ESEEM spectra recorded near g_z and g_x (and simulations to be discussed below) for [^{15}N]heme $Mb^{15}N_3$. Most frequency components in the data are assigned to the proximal imidazole coupling according to the following. The ESEEM spectra of low-spin iron porphyrin complexes such as Fe(III)[^{15}N]TPP([^{14}N]pyridine)/(RO^-) and [^{15}N]-heme MbOH do not contain contributions from the [^{15}N]-pyrroles (Magliozzo & Peisach, 1992). As the magnitude of the [^{15}N]pyrrole couplings is not expected to be much different in [^{15}N]heme $Mb^{15}N_3$ (Mulks et al., 1979), no spectral components are expected nor are any assigned to these sites. Furthermore, the directly coordinated ^{14}N of imidazole is the ligand giving rise to the ESEEM spectrum of a low-spin complex, the remote nitrogen being too weakly coupled to contribute any modulations (Mims & Peisach, 1989; Magliozzo & Peisach, 1992).

The spectra for [^{15}N]heme $Mb^{15}N_3$ shown in Figure 1A,C, do, however, contain components at the Larmor frequency of ^{15}N [1.1 MHz in the spectrum recorded at 2582 Gauss (g = 2.43) and 1.6 MHz at 3615 Gauss (g = 1.74)]. These components, absent from spectra recorded for a sample of MbN_3 containing all ^{14}N (not shown), arise from weakly coupled ^{15}N of the azide ligand (Dikanov & Astashkin, 1989).[4]

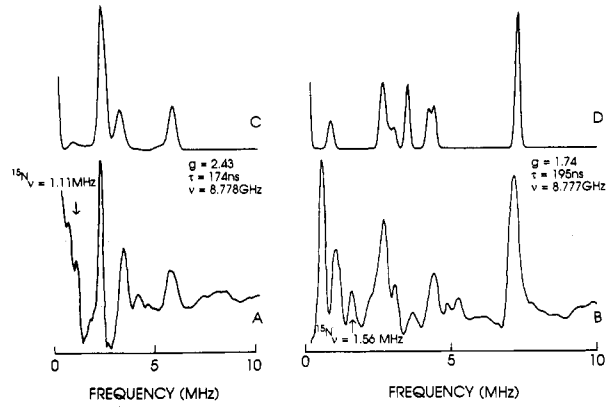

FIGURE 1: (A, B) ESEEM spectra of [^{15}N]heme Mb$^{15}N_3$. (C, D) ESEEM simulations for the directly coordinated nitrogen of the proximal imidazole. Simulation parameters are given in Table I. The experimental g values, microwave frequencies, and the values of τ are given in the figure. Arrows indicate the Larmor frequencies for ^{15}N. The simulation of peak intensities at $g = 2.43$ is better than at other experimental g values. This result is due in part to the "tau" effects that give suppression and enhancement of modulation components (Mims & Peisach, 1989). The simulation functions are less sensitive to these effects than are the experimental data. The component at approximately 4.2 MHz in the spectrum at $g = 2.43$ is present in the time domain function for the simulation but is too broad in the Fourier transform presented here and therefore does not appear above the baseline. The intensity at 5 MHz in the spectrum in B is an instrumental artifact. The lines due to ^{15}N are not included in the simulations of spectra for [^{15}N]heme Mb$^{15}N_3$).

Thus, all lines in these two spectra except those occurring at the ^{15}N Larmor frequency arise from the proximal imidazole nitrogen. Better resolution of the low-frequency components was seen in other ESEEM spectra obtained at another τ value but also at $g = 2.43$ (not shown), in which a low-intensity peak at the ^{15}N Larmor frequency plus a shallow peak at approximately 0.8 MHz were seen. The latter, which was poorly resolved in the spectrum in Figure 1A, is assigned as a component of the set of lines arising from the coordinated ^{14}N of the proximal imidazole and is duplicated in the simulation presented for the $g = 2.43$ data. Some ambiguity in the simulation of the ESEEM spectrum at $g = 1.7$ is evident in the frequency range below 1 MHz. That neither of the components below 1 MHz arises from ^{15}N nuclei was ruled out by noting the presence of the same components in spectra from a sample of all ^{14}N-containing MbN_3 (not shown). Only one component was generated in this frequency range in simulations using a wide range of hyperfine and quadrupole coupling parameters though increasing the anisotropy of the hyperfine coupling did introduce a splitting of the component at 0.9 MHz (not shown).

The spectra for [^{15}N]heme Mb$^{15}N_3$ recorded near g_z and g_x (Figure 1) are similar to those of [^{15}N]heme MbOH (Magliozzo & Peisach, 1992), though the nitrogen nuclear hyperfine coupling is smaller and the nuclear quadrupole coupling constant is larger for the azide complex compared to the values found for MbOH. Table I summarizes these results along with parameters for the complexes presented below. The nitrogen nuclear hyperfine coupling for the proximal imidazole nitrogen in [^{15}N]heme Mb$^{15}N_3$ is essentially isotropic, with a_{iso} equal to 4.4 MHz. The anisotropy in the hyperfine coupling values needed to fit the spectra at different magnetic field values gives an axial form ($A_y = A_x$) with the smallest value ($|A_z|$) occurring for the hyperfine principal axis component aligned near g_z. For example, the highest frequency component in the ESEEM spectrum at $g = 2.43$ occurs at 5.8 MHz but occurs at 7.22 MHz in the spectrum recorded at $g = 1.74$. This frequency change was simulated by assigning the hyperfine element $|A_z|$ a value 1.6 MHz smaller than the value assigned to $|A_x|$.

The small values for the Euler rotation angles in the results for MbN_3 suggest near alignment of the hyperfine, nuclear quadrupole, and g tensor principal axis directions. The Euler angle β for the nqi principal axis system has a small value, consistent with Q_{zz} being close to the heme normal. [The value of $\sim 20°$ for β can be accounted for by the misalignment of g_z with respect to the heme normal ($\sim 10°$) (Helcké et al., 1968; Hori, 1971) and some misalignment of Q_{zz} with respect to the lone pair orbital direction or even a misalignment of the axial bond direction with respect to the heme normal.] If the direction of Q_{yy} is assumed to be perpendicular to the imidazole ring plane (Ashby et al., 1978), collinearity of this axis with g_y (a small value for the angle α) is consistent with the orientation of the imidazole demonstrated by X-ray crystallography of myoglobin (Kuriyan et al., 1986).

Figure 2 shows ESEEM spectra and simulations for the proximal imidazole nitrogen in [^{15}N]heme MbC^{14}N. In order to rule out the presence of coupling components arising from ^{14}N of cyanide, spectra for MbC^{14}N (not shown) and MbC^{15}N were compared. A set of "ratio spectra", which are the Fourier transforms of the quotients of modulation envelopes for isotopically substituted pairs of samples (Mims & Peisach, 1989), demonstrated that shallow components due to ^{14}N of the cyanide ligand appeared under experimental conditions different from those used for collection of the data presented here.

The spectra for [^{15}N]heme MbCN contain the four components whose characteristics indicate cancellation of the hyperfine interaction and the Zeeman interaction in one of the electron spin manifolds (Mims & Peisach, 1989). Therefore, the nqi parameters are calculated with greater accuracy here than in the preceding example. The values given in Table I ($e^2Qq = 2.5$ MHz; $\eta = 0.3$) are similar to those reported for the proximal imidazole nitrogen in MbOH (Magliozzo & Peisach, 1992), demonstrating that the modulations in the spectrum for MbCN arise from the directly coordinated axial nitrogen. The calculated a_{iso} value was 2.23 MHz and the anisotropy in the terms for the hyperfine interaction was similar in form to the other cases. The g_z axis direction is near the heme normal in MbCN also, but the in-plane g tensor axes are very close to Fe–$N_{pyrrole}$ vectors and are inverted compared to those in MbN_3 (Peisach et al., 1971; Shulman et al., 1971; Rhynard et al., 1979). The new orientation of g_y was not evident in the Euler rotation angles for the nqi principal axis system as a value of zero was satisfactory for both α and γ.

The ESEEM spectra of MbRS (Figure 3) were recorded for samples prepared from native metMb as the contributions from axial and pyrrole ^{14}N sites could be treated separately by referring to previously published results (Peisach et al., 1979). The analysis of ESEEM spectra for low-spin Fe(III)-TPP and Fe(III)PPIX model complexes containing an axial

[4] The ^{15}N site giving rise to these components is most likely the weakly coupled β- or γ-nitrogen of the azide ligand and not the directly coordinated nitrogen. This suggestion is based on the expected similarity between the directly bound nitrogen of azide and the directly coordinated nitrogen of [^{15}N]pyridine in a low-spin Fe(III)TPP complex, the latter having previously been shown to give only very shallow modulations in ESEEM spectra (Magliozzo & Peisach, 1992). Furthermore, calculations have shown that modulation depths in ESEEM spectra are very shallow for ^{15}N ($I = 1/2$) sites having isotropic hyperfine interactions in the range of 4–5 MHz (Magliozzo et al., 1987). These phenomena also explain the absence of contributions from the [^{15}N]pyrrole nitrogens to the ESEEM spectra of the Mb complexes studied here.

Table I: Nitrogen Nuclear Hyperfine and Quadrupole Coupling Parameters for Low-Spin Myoglobin Complexes

	hyperfine coupling (MHz)				quadrupole coupling (MHz)	
	A_x	A_y	A_z	a_{iso}[a]	e^2Qq	η[b]
(A) Directly Coordinated Nitrogen of Proximal Imidazole						
[^{15}N]heme Mb^{15}N$_3$	4.6 (α, β, γ = 0°, 10°, 0°)[c]	4.6	3.0	4.4	3.2 (α, β, γ = 0°, 23°, 0°)[c]	0.1
[^{15}N]heme MbCN	2.6 (α, β, γ = 0°, 15, 0°)	2.6	1.5	2.2	2.5 (α, β, γ = 0°, 5°, 0°)	0.3
Mb(β-mercaptoEtOH)	2.6 (α, β, γ = 0°, 7°, 0°)	2.6	1.4	2.2	2.5 (α, β, γ = 0°, 18°, 0°)	0.3
[^{15}N]heme MbOH[d]	5.5 (α, β, γ = 0°, 7°, 0°)	5.5	4.2	5.1	2.3 (α, β, γ = 0°, 13°, 0°)	0.1
(B) Pyrrole Nitrogens						
Mb(β-mercaptoEtOH)				5.1	2.15 (α, β, γ = 0°, 40°, 0°)	0.5
				4.6	2.15 (α, β, γ = 0°, 40°, 0°)	0.5
				4.1	2.15 (α, β, γ = 0°, 50°, 0°)	0.5

[a] All terms are negative; $a_{iso} = {}^1/_3[A_x + A_y + A_z]$. [b] $\eta = (q_{xx} - q_{yy})/q_{zz}$. [c] Euler rotation angles to g tensor reference frame. [d] Taken from Magliozzo and Peisach (1992).

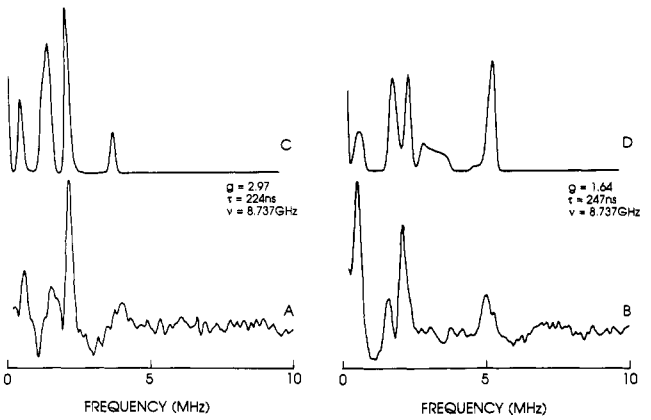

FIGURE 2: (A, B) ESEEM spectra of [^{15}N]heme MbCN. (C, D) Fourier transforms of ESEEM simulations for the directly coordinated nitrogen of the proximal imidazole. Simulation parameters are given in Table I. The experimental g values, microwave frequencies, and the values of τ are given in the figure.

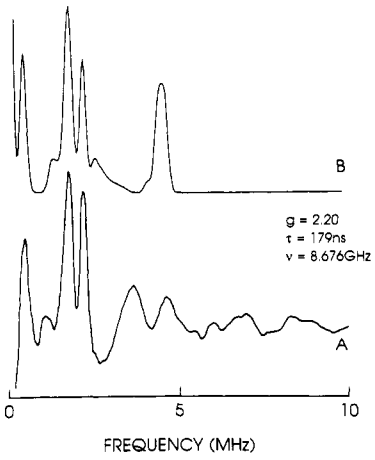

FIGURE 3: (A) ESEEM spectrum of MbRS. (B) ESEEM simulations for the directly coordinated nitrogen of the proximal imidazole. Simulation parameters are given in Table I. The experimental g value, microwave frequency, and the value of τ are given in the figure. The line at 3.7 MHz is a [^{14}N]pyrrole modulation frequency.

thiolate plus an axial *imino* or *amino* nitrogen ligand demonstrated that (1) it is the directly coordinated axial nitrogen that gives rise to the sharp lines, and (2) the [^{14}N]-pyrrole sites have negligible contributions that overlap

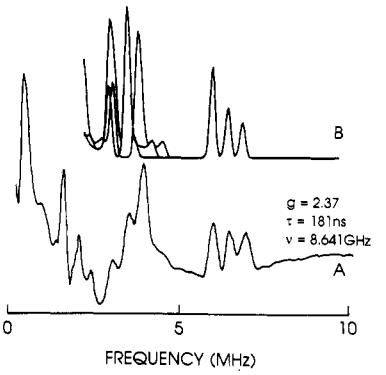

FIGURE 4: (A) ESEEM spectrum of MbRS. (B) ESEEM simulations for [^{14}N]pyrrole sites. Three sets of coupling parameters given in Table I were used to generate the simulations in B, which are presented as a composite of three simulations. The experimental g value, microwave frequency, and the value of τ are given in the figure.

with those arising from the directly coordinated axial nitrogen for most choices of experimental conditions (Peisach et al., 1979). For MbRS (Figure 3), three sharp components at 0.43, 1.73, and 2.15 MHz arise from the proximal imidazole nitrogen (Peisach et al., 1979). These components are similar to those in the spectra for MbCN and again reflect a nitrogen nuclear hyperfine coupling whose magnitude satisfies the exact cancellation condition. The line at 3.66 MHz is one component from a complex pattern due to [^{14}N]pyrrole couplings that are resolved better in a spectrum presented below.

The coupling parameters for the proximal imidazole nitrogen calculated by simulation of spectra for MbRS, excluding the 3.66-MHz line (Figure 4), are given in Table I (a_{iso} = 2.19 MHz; e^2qQ = 2.5 MHz; η = 0.3). The nqi parameters are similar to those for MbOH and MbCN. All Euler rotation angles are small, as in the other cases. Furthermore, based on the small value for the Euler rotation angle, β, for the nqi principal axis system, the $g_{max} = g_z$ direction in MbRS remains close to the heme normal. This localization of a g tensor axis direction can usually be achieved only by single-crystal EPR experiments. The e^2Qq value calculated here for the proximal imidazole nitrogen in MbRS agrees with a value previously reported (Flanagan et al., 1987) from a two-pulse ESEEM study in which "anomalous" nuclear quadrupole axes were assigned for this site. Anomalous nqi axes for the *imino* nitrogen indicate that Q_{zz} is no longer associated with the lone pair donor orbital direction, as occurs for example upon

protonation of the *imino* site of imidazole (Ashby et al., 1978). If anomalous nqi axes occurred in the coordinated nitrogen of the proximal imidazole in MbRS, the direction of Q_{zz} would no longer be near the direction of g_{max} (taken along the heme normal) but would instead make a large angle with this axis. Simulation of the three-pulse spin echo modulation data here could not, however, be achieved using large values for the Euler rotation angle β. Thus, no evidence for anomalous axes could be substantiated in these results. Furthermore, the three-pulse ESEEM data, in which the zero-field nqi frequency components are clearly resolved (Figure 3) are only consistent with a value for η smaller than 0.632 (Flanagan et al., 1988).

Pyrrole Nitrogen Couplings. The nuclear hyperfine couplings for the pyrrole nitrogens in MbCN and MbN_3 were reported to be near 6 MHz in an ENDOR study (Mulks et al., 1979). An analysis of the modulation components in ESEEM spectra arising from the pyrrole nitrogens for these two low-spin forms is not presented in any detail here though estimates for the hyperfine couplings from ESEEM data were in agreement with the previously reported values. The small inequivalence resolved in the ENDOR experiments, however, was not seen in ESEEM spectra for [^{14}N]heme MbN_3 or [^{14}N]heme MbCN.

The pyrrole nitrogen couplings in MbRS have been examined in detail here because of the resolution found in ESEEM spectra recorded near g_{max}. Figure 4 shows an example recorded at $g = 2.37$. The components centered near 3 and 6 MHz are assigned to the [^{14}N]pyrrole sites on the basis of the presence of analogous modulations in ESEEM spectra of the model complex Fe(III)PPIX(RS)/([^{15}N]-imidazole) (Peisach et al., 1979) though no multiplicity was resolved before (Peisach et al., 1979). Three sets of coupling parameters (Table I) were used to simulate the [^{14}N]pyrrole contributions in the high-frequency region of the data shown in Figure 4B. The values of a_{iso} required to give the three highest frequency components were 5.1, 4.6, and 4.1 MHz, using nqi parameters estimated by simulation (not shown) of the pyrrole contributions in spectra of the model complex Fe(III)PPIX(RS^-)/([^{15}N]imidazole) (Peisach et al., 1979). The nqi parameters are similar to those reported for the pyrrole nitrogens in MbOH (Magliozzo & Peisach, 1992). The relative intensity of the highest frequency components suggests that two nitrogens with equal coupling give rise to the more intense peak at 6.0 MHz and a single nitrogen gives rise to each of the higher frequency lines at 6.5 and 7.0 MHz. The simulation presented, however, is a composite generated using three sets of coupling parameters without any multiplicity for any set. In cases where the exact cancellation condition is met, the height of peaks in the Fourier transforms is related to the number of nuclei with equivalent coupling (McCracken et al., 1988, 1989; Mims & Peisach, 1989). But here, for pyrrole nitrogens with stronger hyperfine couplings, the multiplication of simulated modulation functions for two equivalent nitrogens did not lead to differences in the Fourier transforms. [The simulation programs can incorporate multiple couplings by squaring (or raising to higher powers) the modulation function generated for a single site.] The results for the pyrrole couplings in MbRS should incorporate two equal and one each of two additional sets of coupling parameters, however, since it is unlikely that the ESEEM components arise from only three of the four pyrrole sites.

Several components near 3 MHz are generated in simulations using the [^{14}N]pyrrole parameters given in Table I. The position and intensities of these components depends on the magnitude of nqi parameters as well as on the Euler rotation angles for the nqi principal axes. A rigorous simulation of these is not feasible, mainly because there is no unambiguous way to assign a 3-MHz line (or lines) to its correct partner near 6 MHz for one particular nitrogen. The hyperfine couplings are, however, evaluated with confidence in spite of an incomplete treatment, since the frequency of the lines near 6 MHz are most sensitive to the value of a_{iso} and are much less sensitive to the quadrupole parameters and Euler rotation angles. The a_{iso} values for the [^{14}N]pyrroles in MbRS are all smaller than the average values reported for MbN_3 and MbCN (Mulks et al., 1979).

DISCUSSION

Origin of Hyperfine Coupling. The nuclear hyperfine coupling parameters for the directly bound ^{14}N of the proximal imidazole in three low-spin Mb complexes reveal a trend in the values of their isotropic components (a_{iso}) that varies from 4.4 MHz for the azide to 2.2 MHz for the cyanide and thiolate forms. These changes may be analyzed from the point of view that the CN^- and RS^- ligands yield complexes in which the axial imidazole interaction is weakened, compared to that occurring in MbOH and MbN_3, due to new structural and or electronic features that accompany the binding of these anions. For example, either a *trans* effect, a distortion near the iron such as its movement out of the porphyrin plane, or a redistribution of unpaired electron spin density in the iron–ligand orbital system alone or in combination could contribute to a weakened hyperfine coupling interaction. The first two effects could involve changes in the length of the imidazole–iron bond. The third effect would change the "dipolar" or effective distance from the unpaired electron to the coupled nitrogen (but would not necessarily change the actual bond length) (Schweiger, 1982; Cornelius et al., 1990).

The low-spin iron orbital system has the electron configuration d_{xy}^2, d_{xz}^2, d_{yz}^1, according to the orbital coefficients that result from a crystal field analysis applied to the t_{2g} set of d orbitals (Griffith, 1957; Taylor, 1977; Bohan, 1977; Muhoberac, 1984). One of the d–π orbitals situated perpendicular to the porphyrin plane contains most of the unpaired spin density with the other d orbitals sharing small amounts through spin orbit coupling, while the e_g orbitals are considered to be empty. In Mb, the coordinated *imino* nitrogen of the proximal imidazole, considered to be sp^2 hybridized, has a p–π orbital oriented perpendicular to the heme normal that may be oriented parallel to the partially filled d orbital. The position of the imidazole, presumably invariant in various Mb complexes, fixes this nitrogen π orbital in an orientation that nearly eclipses an Fe–$N_{pyrrole}$ vector (Kuriyan et al., 1986, and references therein). Though overlap between the p–π and the half-filled d–π orbital could facilitate direct transfer of unpaired spin into the axial ligand, experimental evidence against such a mechanism for the origin of the nitrogen nuclear hyperfine coupling interaction is contained in the following: an ESEEM study of low-spin iron porphyrin model complexes containing nitrogen and oxygen ligand pairs showed that the value of a_{iso} for the axial *amino* nitrogen in Fe(III)TPP-(butylamine)(OR^-), 4.0 MHz, was nearly as strong as that for the directly bound *imino* nitrogen of pyridine or imidazole in similar complexes (a_{iso} = 4.6 and 5.1 MHz, respectively) (Magliozzo & Peisach, 1992). A close agreement between amine and imidazole couplings was also found in ESEEM spectra of Fe(III)PPIX(propylamine)(RS^-) and Fe(III)PPIX(imid)/RS^- (as found in MbRS) (Peisach et al., 1979). Since the amine nitrogen is not likely to participate in π bonding while the *imino* nitrogen ligands of the

heterocycles will, these results are taken as evidence that the π system of the nitrogen ligand does not support a major part of the nuclear hyperfine interaction through d–π p–π spin transfer. Additional evidence that the nitrogen nuclear hyperfine coupling does not occur through spin transfer into the π system has been suggested by the following: The sign of a_{iso} for the nuclear hyperfine interaction at the axial nitrogen in low-spin heme complexes was reported to be negative (Scholes et al., 1986) while in ^{14}N p–π radicals, the values are positive (Carrington & McLachlan, 1967). A coupling mechanism involving spin transfer into the proximal imidazole nitrogen in a low-spin Mb complex would be expected to give a positive value for a_{iso}, as this interaction can presumably lead to a spin system analogous to that of the nitrogen radical. It was found, however, that A_z was the weakest hyperfine coupling term (Scholes et al., 1986), i.e., the value occurring along the axis direction parallel to the iron–nitrogen bond (this being the direction selected by EPR experiments near g_z for low-spin heme). The strongest hyperfine coupling term should occur in this direction, along a vector joining the electron and the nitrogen nucleus. Therefore, it was concluded that a dipolar interaction between nitrogen and the metal unpaired electron causes spin polarization in the axial nitrogen of low-spin Fe(III)P complexes and thereby yields a negative value for a_{iso} (Scholes et al., 1986).

In all low-spin Fe(III)P complexes examined by ESEEM, $|A_z|$ was found to be the smallest term, and a similar coupling mechanism is suggested to operate throughout. Negative values for nitrogen nuclear hyperfine couplings have also been assigned in other metal–nitrogen systems (Cornelius et al., 1990; Rudin et al., 1982). It should be noted that according to the g tensor axis orientation determined by single-crystal EPR (Helcké et al., 1968) and single-crystal Mossbauer spectroscopy of MbN_3 (Harami, 1979), the p–π orbital of the proximal imidazole nitrogen is not optimally oriented for good overlap with the half-filled d–π orbital, lending credence to the suggestion that no spin transfer occurs (see below). Direct spin transfer through the iron–nitrogen σ bond is not implicated as a source of hyperfine coupling for axial nitrogen since the d_{z^2} orbital is considered to be empty for low-spin iron.

Having ruled out direct spin transfer as the dominant mechanism leading to nitrogen nuclear hyperfine coupling in the proximal imidazole, the trend in a_{iso} values must be discussed in some other context. For example, a structural *trans* effect in MbCN or MbRS, absent from MbN_3 and MbOH, could lead to the weakened hyperfine coupling. In small molecule complexes, a structural *trans* effect due to thiolate ligands has been noted by X-ray crystallographic analyses of bond lengths in Co(III) complexes, but the effect was not seen in Cr(III) complexes (Elder et al., 1973). No structural effect is apparent in a comparison of the Fe–N_{axial} bond lengths for Fe(II)TPP complexes with bisimidazole axial ligation vs imidazole/thioether ligation (Mashiko et al., 1981). A strong argument against such an effect in low-spin Mb is the constancy of the nuclear quadrupole coupling constants, e^2Qq, for the coordinated nitrogen of the proximal imidazole in the CN^-, RS^-, and OH^- forms (Table I).

The value of e^2Qq is related to the nitrogen lone pair donor orbital population (Ashby et al., 1978, 1980) and thus reflects the strength of the nitrogen base–Lewis acid interaction between the proximal imidazole and the metal ion. Large values ($\approx$3 MHz) are consistent with poor lone pair donation and would indicate electron populations in the donor orbital close to 2 (Ashby et al., 1978; Cornelius et al., 1990). The values near 2.5 MHz found for MbOH, MbCN, and MbRS are within the rather narrow range reported for many different complexes including crystalline $Zn(II)(imid)_2(Cl)_2$ (Ashby et al., 1978). If the small hyperfine coupling in MbCN and MbRS were due to a *trans* effect or other distortion that reduced imidazole to iron overlap, it would have been accompanied by a large e^2Qq value for this nitrogen. [For MbN_3, a large e^2Qq value was in fact found, though in this complex it occurs along with a large value for the nitrogen nuclear hyperfine interaction (see below).]

It therefore seems likely that the reduction in proximal imidazole coupling in MbCN and MbRS arises from a redistribution of the unpaired electron spin density due to covalency between iron and sixth ligands that does not occur in MbOH or MbN_3. Any reduction of the total spin density in iron orbitals would give smaller a_{iso} values, whatever the mechanism for electron nuclear coupling. An electron acceptor role for CN^- and RS^- would account for the effect, so long as the unpaired electron were involved in the delocalization. The thiolate ligand in MbRS can utilize empty d orbitals for this interaction while, for CN^-, empty π^* orbitals are available (Fallon & Gatehouse, 1974; Redhouse, 1973; Johnson et al., 1991). Direct evidence for spin delocalization into the cyanide ligand is found in the large value (5 MHz) of the nuclear hyperfine coupling for ^{15}N in Mb$C^{15}N$ (Mulks et al., 1979). An analogous coupling ($\sim$3.9 MHz) was estimated for ^{14}N in Mb$C^{14}N$ by a ratio analysis of ESEEM spectra (not shown) described above. No relevant coupling data for MbRS are available though significant covalency has been noted for the sulfide ligand in an Fe(III)P(HS^-) complex (English et al., 1984) and for the thiophenolato ligands in a Co(II) complex (Fukui et al., 1992).

No correlation is apparent between the trend in hyperfine couplings for the low-spin forms and the tetragonal and rhombic splittings calculated according to the crystal field analysis (Blumberg & Peisach, 1971; Taylor, 1977; Bohan, 1977; Muhoberac, 1984) as MbOH and MbRS have very similar tetragonal and rhombic splitting parameters yet very different proximal imidazole hyperfine couplings, while MbCN has a very small rhombicity with a hyperfine coupling similar to that of MbRS. (The tetragonal splitting is the difference in energy between the d_{xy} orbital and the average energy of the d_{xz} and d_{yz} orbitals; the rhombic splitting is the difference between the d_{xz} and d_{yz} levels.) The crystal field approach has, however, been successful in correlating structural parameters such as the relative orientation of ligand planes for bisimidazole iron porphyrins with the rhombic and tetragonal splittings (Muhoberac, 1984; Walker et al., 1986; Soltis & Strouse, 1988; Safo et al., 1991, 1992) (see below). What becomes apparent from the results presented is the inadequacy of using a t_{2g} metal-centered basis set alone for a full description of the EPR properties of the various low-spin heme complexes, especially when only one of the axial ligands governs the rhombic axis orientation.

The Unusual Nuclear Quadrupole Coupling Constant for the Proximal Imidazole in MbN_3. The nuclear quadrupole coupling constant for the coordinated nitrogen of the proximal imidazole is expected to be sensitive to axial bond changes in Mb complexes, as stated above, since it depends on the electronic features of the valence shell of the bound nitrogen (Townes & Daily, 1957; Ashby et al., 1978). This parameterr is essentially invariant in all low-spin Mb complexes examined so far, except for MbN_3. The value calculated for MbN_3 seems to be anomalously large (3.2 MHz) as it nearly equals that for the *imino* nitrogen in solid imidazole and in solid L-histidine [3.3 and 3.4 MHz, respectively (Ashby et al.,

1978)]. These imidazole compounds, however, have significant hydrogen bonding interactions at both ring nitrogens, which reduces the quadrupole coupling that would better represent a "free" ligand reference value. The e^2Qq for the *imino* site in *N*-benzylimidazole, a better choice for reference because there is no hydrogen bonding in the solid, is 3.7 MHz (Ashby et al., 1978). Nevertheless, the e^2Qq value for the proximal imidazole nitrogen in MbN_3 suggests a weak σ-donor interaction with Fe(III) in this complex while the a_{iso} value is close to that found in MbOH. Therefore, the "effective" or dipolar distance between the nitrogen nucleus and the unpaired electron is similar to MbN_3 and MbOH, and no large structural rearrangement or significant spin delocalization is evident for MbN_3.

Though the value of e^2Qq is expected to increase with bond length for nitrogen-to-metal bonds, the expected correlation may not always be evident in experiments. In crystalline octahedral Cd(II) and Zn(II) hexaimidazole complexes, the coordinated nitrogen sites yield a single e^2Qq value though metal–nitrogen bond lengths vary up to 0.2 Å within the structures (Ashby et al., 1978). In other complexes, however, two sets of nqr parameters are resolved for two very similar metal–imidazole nitrogen distances, such that e^2Qq values equal to 2.019 and 2.062 MHz correspond to the Zn–N bonds with lengths of 2.001 and 1.997 Å in $Zn(imid)_4(ClO_4^-)_2$ (Ashby et al., 1978). Therefore, though the large e^2Qq value for MbN_3 suggests an elongation of the proximal imidazole-to-iron bond, it should not be taken as conclusive evidence for such a change since a range of bond lengths can apparently give similar nitrogen nuclear quadrupole couplings.

The value of e^2Qq is most easily correlated with effects in the donor orbital (lone pair), though it seemed that clues about π-bonding features for the proximal imidazole might be inferred from this parameter. In fact, the iron–nitrogen π bonds for the proximal imidazole in MbN_3 can be shown to differ from those in the other low-spin forms having what may now be considered typical e^2Qq values (near 2.5 MHz). In model complexes, the coordinated nitrogen in imidazole–Cd(II) or –Zn(II) bonds exhibits e^2Qq values near 2.5 MHz (Ashby et al., 1978) consistent with electron populations in the donor orbital that can be as low as 1.6 electrons. According to a Townes–Dailey model for the nitrogen valence electrons (Townes & Daily, 1949) applied to analyze these parameters (Ashby et al., 1978), the ligand nitrogen recruits electron density from the σ and π orbital system of the heterocycle ring itself to the extent that 60% of the lost electron density can be compensated for. The π system of imidazole could presumably also recover electron density from metal dπ orbitals in an M → L acceptor interaction. Since the electron configuration of low-spin iron gives one filled and one half-filled dπ orbital, the π-bonding interactions for the proximal imidazole nitrogen as well as those for the porphyrin nitrogens could involve either L → M or M → L π donation. The latter interaction is usually not expected to be favorable for imidazole (or pyrrole nitrogens), though a molecular orbital calculation (Satterlee & La Mar, 1975) has demonstrated that d–π overlap with empty imidazole p–π^* orbitals is inherently favored because of the orbital symmetries. Furthermore, it has been noted that imidazole does not act as a π-donor in Fe(III)-$(CN)_5$(imidazole) (Johnson et al., 1991). Thus, M → L donation should not be neglected as a potential interaction in the imidazole–iron system.

The asymmetry in the electronic features of axial ligands in low-spin complexes introduces rhombic axes into the d orbital system that determine the orientation of the filled and half-filled orbital planes. The *g* tensor orientation is then governed by the rhombic axes (along with any asymmetry from the equatorial bonds). The axis orientation may be determined by the combined interactions of both axial ligands or by rhombic axes due only (or mostly) to the anionic or strongest field ligand. Examples for the rotation of the rhombic axes accompanied by rotation of the *g* tensor are found in low-spin Fe(III)P complexes containing thiol/thiolate ligand pairs (Byrn et al., 1983), in two cytochromes *c* (Senn et al., 1980; Keller & Wüthrich, 1978), and in $Fe(III)TPP(imid)_2$ (Soltis & Strouse, 1988). In the cytochromes, the orientation of in-plane axes of the *g* tensor (g_y and g_x) has been correlated with the orientation of the axial sulfur ligand of methionine for two proteins that differ in the geometry of the $-SCH_3$ group and thereby the orientation of rhombic axes (Seen et al., 1980; Keller & Wüthrich, 1978). In the Fe(III)P(thiol/thiolate) complexes, the thiolate, and not the thiol-type sulfur, was found to determine the orientation of the *g* tensor (Byrn et al., 1983).[5] (The bisimidazole complexes are discussed below.)

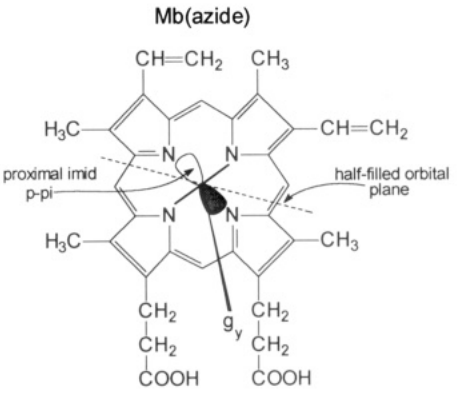

FIGURE 5: Heme in MbN_3 showing the orientation of *g* tensor axes [according to Helcké et al. (1968)] and the projection onto the heme of the proximal imidazole plane as well as the nitrogen p–π orbital. The half-filled orbital plane is indicated according to Byrn et al. (1983).

In MbN_3, the partially filled orbital plane has been assigned to lie between an $Fe–N_{pyrrole}$ vector and a meso carbon plane (Byrn et al., 1983), according to the *g* tensor axes determined from single-crystal EPR (Helcké et al., 1968) and the location of the principal axis of the electric field gradient tensor for ferric iron analyzed by single-crystal Mössbauer spectroscopy (Harami, 1979). It is therefore located *between* the projection onto the heme plane of the p–π orbital directions of both axial nitrogen ligands (Figure 5) (Byrn et al., 1983). According to X-ray structures of Mb (Phillips, 1980; Kuriyan, 1986, and references therein), the proximal imidazole ring plane lies nearly parallel with an $Fe–N_{pyrrole}$ vector direction. Therefore, the p–π imidazole orbital in MbN_3 must have poor overlap with d–π orbitals though it does lie closer to the half-filled orbital plane. This nitrogen π orbital cannot receive π electron density (back-bonding) from the d–π system of iron, and thus a weaker σ overlap and larger e^2Qq might be expected. To generalize these ideas, when the rhombic axes for a low-spin complex are oriented such that overlap between the filled d–π orbital plane and the p–π of the proximal imidazole is favorable, a strong σ donor interaction can be accommodated because it will be accompanied by a back-bonding interaction. These electronic effects are presented schematically in Figure

[5] Note that the rotation of rhombic axes in one direction causes a rotation of the *g* tensor axes in the opposite sense (Oosterhuis & Lang, 1969; Byrn et al., 1983).

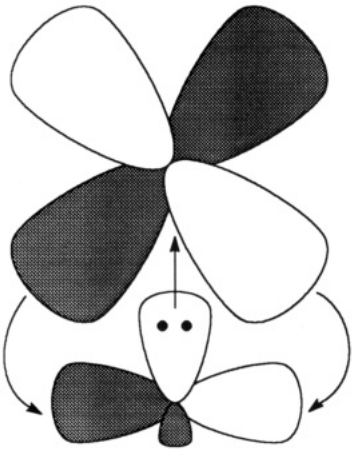

FIGURE 6: Illustration of d–π and p–π orbitals of iron and axial nitrogen showing the M → L back-bonding favored for a filled d–π. L → M donation would be favored for a half-filled d–π.

6. Note that they are illustrated for the p–π of imidazole but might better be represented by π^* for the nitrogen acceptor orbital.

The apparently weak σ donor interaction for the proximal imidazole in MbN_3 may be related to the weak axial ligand field associated with the high-spin–low-spin equilibrium observed for this complex as a function of temperature (Beetlestone & George, 1964; Iizuka & Kotani, 1968; Desbois et al., 1979; Vickery et al., 1975). A structural origin for this phenomenon has not been explained in detail. No unusual features have been reported from resonance Raman spectroscopy of HbN_3 or MbN_3 (Desbois et al., 1979; Henry et al., 1985) that would suggest a large structural change in these forms compared to MbCN though the ESEEM results may be considered evidence for a structural *trans* effect and a lengthening of the proximal imidazole to iron bond. Unfortunately, the interpretation of the Raman spectra lacks an assignment of axial imidazole nitrogen–iron stretching frequencies, and no quantitative comparisons can be made between the ESEEM and Raman results. It is noted here that of two low-spin Fe(III)P model complexes containing axial pyridine plus either CN^- or N_3^- ligands, the azide complex exhibits a longer Fe(III)–pyridine bond (Adams et al., 1979; Scheidt et al., 1983). This result is consistent with the results discussed here for the two analogous Mb complexes. Furthermore, the disruption of the proximal imidazole to iron bond is not without precedent. For example, the α subunits of partially ligated nitrosyl hemoglobin in its low-affinity form provide an example in which the heme is converted to a five-coordinate form (Szabo & Perutz, 1976; Hille et al., 1979; Magliozzo et al., 1987).

For MbCN, an analysis of the iron electric field gradients by Mössbauer spectroscopy of frozen solution samples (Rhynard et al., 1979) is consistent with rhombic axes lying close to the cubic axes (8° from the Fe–$N_{pyrrole}$ vectors) (Figure 7). The location of g_y, according to a single-crystal EPR study (Peisach et al., 1971) and an early NMR study (Shulman et al., 1971), also suggests that the half-filled orbital plane nearly

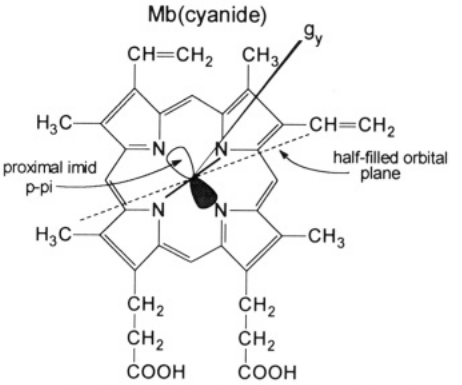

FIGURE 7: Heme in MbCN showing the orientation of g tensor axes [according to Peisach et al. (1971) and Shulman et al. (1971)] and the same proximal imidazole features as in Figure 5. The orientation of the half-filled orbital plane is indicated according to the analysis discussed by Byrn et al. (1983) after Oosterhuis and Lang (1969).

eclipses an Fe–$N_{pyrrole}$ vector.[6] Therefore, the p–π orbital of the proximal imidazole in MbCN must be located closer to the *filled* d–π orbital plane, potentiating π back-bonding and a better σ donor interaction, giving a more typical value for e^2Qq. Thus, changes in the nuclear quadrupole interaction for the axial nitrogen in two low-spin species, MbCN and MbN_3, seem to be correlated with changes in the orientation of the g tensor and with π-bonding features. For MbRS, the rhombic axes (and thus the in-plane g tensor axes) should be oriented similar to those in MbCN since a strong σ donor interaction occurs. The ESEEM results have thus enabled a tentative assignment of the g tensor in a low-spin complex, the g_z axis having been localized according to the Euler rotation angle for the nqi axis Q_{zz}, and the in-plane axes being indirectly fixed according to the value of e^2Qq.

Pyrrole Nitrogen Couplings. The resolution of a set of pyrrole nitrogen nuclear hyperfine couplings in ESEEM spectra is noteworthy for the MbRS complex though some inequivalence in hyperfine coupling interactions was reported in ENDOR studies of pyrrole sites in other low-spin Mb forms (Mulks et al., 1979; Scholes et al., 1986). A structural inequivalence arises partly from "ruffling" of the macrocycle structure and is correlated with electronic features in examples of two crystal forms of the low-spin model complex Fe(III)-$P(imid)_2$ (Scheidt & Reed, 1981). In one crystal form, the plane containing parallel imidazole rings eclipses an Fe–$N_{pyrrole}$ direction. The electronic overlap along the axial p–π orbital directions acts to localize the unpaired electron in the plane perpendicular to the rings. The difference in occupancy of the half-filled and filled orbital planes then leads to a difference in the potential π overlap for opposite pairs of pyrrole nitrogens (Walker et al., 1986): The pair of pyrroles having p–π orbitals nearer the half-filled orbital plane participate in a π-donor interaction and are found to have shortened bond lengths, while the opposite pyrrole nitrogens cannot donate electron density into the filled d–π orbital orbital plane (and have longer bonds). The difference in Fe–$N_{pyrrole}$ bond lengths is absent when the rhombic axes orient the filled and half-filled orbital planes *between* the nitrogens (toward the *meso* carbon positions), as occurs in the second crystal form of the model complex (Walker et al., 1986). These structural effects are also correlated with the rhombicity calculated in the crystal field analysis based on the EPR spectra of the two crystalline species. The rhombic splittings vary as expected, from large for the complex having the Fe–$N_{pyrrole}$ vector eclipsed by the ligand planes, to small for the other form. These two

[6] According to recent NMR results at room temperature (Emerson & La Mar, 1990a,b), the g tensor axes for MbCN in solution are the same as those determined for MbN_3 by single-crystal EPR (Helcké et al., 1968). This result disagrees with the g tensor axis orientation presented by Peisach et al. (1971) from a single-crystal EPR study of MbCN and by Shulman et al. (1971) in an earlier NMR study and disagrees with the orientation of rhombic axes determined by Mossbauer spectroscopy of MbCN in frozen solution (Rhynard et al., 1979).

structures, though they represent extremes in rhombic symmetries, illustrate an important correlation between structural and electronic features that depend on the orientation of the rhombic axes (g tensor). A similar analysis of Fe(III)P bisimidazole complexes is presented by Soltis and Strouse (1988).

These observations suggest that insofar as dipolar coupling mechanisms contribute to the hyperfine interactions for the $N_{pyrrole}$ sites, the a_{iso} values should be correlated with the orientation of the rhombic axes (g tensor) for any low-spin species. Therefore, the large inequivalence for the pyrroles in MbRS suggests these axes are oriented toward the Fe–$N_{pyrrole}$ vectors. In this arrangement, the filled d–π plane could be oriented over the p–π of the proximal imidazole, leading to the typical e^2Qq values discussed above.

Since the asymmetry in pyrrole couplings in MbRS is greater than a pairwise inequivalence, there are other structural or electronic factors involved. For example, the in-plane g axes may lie far enough away from the heme plane to introduce asymmetry in the nitrogen couplings. The latter would occur with a tilt of g_z away from a direction perpendicular to the pyrrole plane. The misalignment of the Q_{zz} and g_z axes in MbRS indicated by the Euler rotation angle ($\beta = 18°$) may be evidence for such a misalignment of g_z with respect to the heme normal.

REFERENCES

Adams, K. M., Rasmussen, P. G., Scheidt, W. R., & Hatano, K. (1979) *Inorg. Chem. 18*, 1892–1899.

Ascoli, F., Rossi-Fanelli, M. R., & Antonini, E. (1981) *Methods Enzymol. 76*, 77–86.

Ashby, C. I. H., Cheng, C. P., & Brown, T. L. (1978) *J. Am. Chem. Soc. 100*, 6057–6067.

Ashby, C. I. H., Paton, W. F., & Brown, T. L. (1980) *J. Am. Chem. Soc. 102*, 2990–2998.

Beetlestone, J., & George, P. (1964) *Biochemistry 3*, 707–714.

Blumberg, W. E., & Peisach, J. (1971) in *Probes of Structure and Function of Macromolecules and Membranes* (Chance, B., Yonetani, T., Mildvan, A. S., Eds.) Vol. II, pp 231–239, Academic Press, NY.

Bohan, T. L. (1977) *J. Magn. Reson. 26*, 109–118.

Byrn, M. P., Katz, B. A., Keder, N. L., Levan, K. R., Magurany, C. J., Miller, K. M., Pritt, J. W., & Strouse, C. E. (1983) *J. Am. Chem. Soc. 105*, 4916–4922.

Carrington, A., & McLachlan, A. D. (1967) in *Introduction to Magnetic Resonance*, pp 111–112, Harper & Row, New York.

Chevion, M., Peisach, J., & Blumberg, W. E. (1977) *J. Biol. Chem. 252*, 3637–3645.

Cornelius, J., McCracken, J., Clarkson, R. B., Belford, R. L., & Peisach, J. (1990) *J. Phys. Chem. 94*, 6977–6982.

Desbois, A., Lutz, M., & Banerjee, R. (1979) *Biochemistry 18*, 1510–1518.

Dikanov, S. A., & Ashtashkin, A. V. (1989) in *Advanced EPR, Applications in Biology & Biochemistry* (Hoff, A. J., Ed.) pp 59–117, Elsevier, Amsterdam.

Elder, R. C., Florian, L. R., Lake, R. E., & Yacynych, A. M. (1973) *Inorg. Chem. 12*, 2690–2699.

Emerson, S. D., & La Mar, G. (1990a) *Biochemistry 29*, 1545–1556.

Emerson, S. D., & La Mar, G. (1990b) *Biochemistry 29*, 1556–1566.

English, D. R., Hendrickson, D. N., & Suslick, K. S. (1984) *J. Am. Chem. Soc. 106*, 7258–7259.

Eglinton, D. G., Gadsby, P. M. A., Sievers, G., Peterson, J., & Thomson, A. J. (1983) *Biochim. Biophys. Acta 742*, 648–658.

Fallon, G. D., & Gatehouse, B. M. (1974) *J. Chem. Soc., Dalton Trans.*, 1344–1347.

Finzel, B. C., Poulos, T. L., & Kraut, J. (1984) *J. Biol. Chem. 259*, 13027–13036.

Flanagan, H. L., & Singel, D. J. (1987) *J. Chem. Phys. 87*, 5606–5616.

Flanagan, H. L., Gerfen, G. L., Lai, A., & Singel, D. J. (1988) *J. Chem. Phys. 88*, 2162–2168.

Fukui, K., Kojima, N., & Ohya-Nishiguchi, H. (1992) *Inorg. Chem. 31*, 1338–1344.

Gibson, J. F., & Ingram, D. J. E. (1957) *Nature (London) 180*, 29.

Gibson, J. F., Ingram, D. J. E., & Schonland, D. (1958) *Discuss. Faraday Soc. 26*, 72–80.

Griffith, J. S. (1957) *Nature (London) 180*, 30.

Harami, T. (1979) *J. Chem. Phys. 71*, 1309–1318.

Helcke, G. A., Ingram, D. J. E., & Slade, E. F. (1968) *Proc. R. Soc. London, Ser. B 169*, 275–288.

Henry, E. R., Rousseau, D. L., Hopfield, J. J., Noble, R. W., & Simon, S. R. (1985) *Biochemistry 24*, 5907–5918.

Hille, R., Olson, J. S., & Palmer, G. (1979) *J. Biol. Chem. 254*, 12110–12120.

Hori, H. (1971) *Biochim. Biophys. Acta 251*, 227–235.

Iizuka, T., & Kotani, M. (1969) *Biochim. Biophys. Acta 181*, 275–286.

Iizuka, T., & Morishima, I. (1974) *Biochim. Biophys. Acta 371*, 1–13.

Jiang, F., McCracken, J., & Peisach, J. (1990) *J. Am. Chem. Soc. 112*, 9035–9044.

Johnson, C. R., Jones, C. M., Asher, S. A., & Abola, J. E. (1991) *J. Inorg. Chem. 30*, 2120–2129.

Keller, R. M., & Wüthrich, K. (1978) *Biochem. Biophys. Res. Commun. 83*, 1132.

Kotani, M. (1961) *Prog. Theor. Phys. Suppl. 17*, 4–13.

Kuriyan, J., Wilz, S., Karplus, M., & Petsko, G. A. (1986) *J. Mol. Biol. 192*, 133–154.

Lucken, E. A. C. (1969) in *Nuclear Quadrupole Coupling Constants*, pp 217–248, Academic Press, London.

Magliozzo, R. S., & Peisach, J. (1992) *Biochemistry 31*, 189–199.

Magliozzo, R. S., McCracken, J., & Peisach, J. (1987) *Biochemistry 26*, 7923–7931.

Mashiko, T., Reed, C. A.; Haller, K. J., Kastner, M., & Scheidt, W. R. (1981) *J. Am. Chem. Soc. 103*, 5758–5767.

Mathews, F. S., Czerwinski, E. W., & Argos, P. (1979) in *The Porphyrins* (Dolphin, D., Ed.) Vol. VIIB, pp 108–146, Academic Press, New York.

McCracken, J., Peisach, J., & Dooley, D. M. (1987) *J. Am. Chem. Soc. 109*, 4064, 4072.

McCracken, J., Pember, S. O., Benkovic, S. J., Villafranca, J. J., Miller, R. J., & Peisach, J. (1988) *J. Am. Chem. Soc. 110*, 1069–1074.

McCracken, J., Cornelius, J. B., & Peisach, J. (1989) in *Pulsed EPR: A New Field of Applications* (Keijzers, C. P., Reijerse, E. J., & Schmidt, J., Eds.) pp 156–161, North Holland, Amsterdam.

Mims, W. B., & Peisach, J. (1978) *J. Chem. Phys. 69*, 4921–4929.

Mims, W. B., & Peisach, J. (1979) in *Biological Applications of Magnetic Resonance* (Shulman, R. G., Ed.) pp 221–269, Academic Press, New York.

Mims, W. B., & Peisach, J. (1989) in *Advanced EPR, Applications in Biology and Biochemistry* (Hoff, A. J., Ed.) pp 1–57, Elsevier, Amsterdam.

Muhoberac, B. B. (1984) *Arch. Biochem. Biophys. 233*, 682–697.

Mulks, C. F., Scholes, S. P., Dickinson, L. C., & Lapidot, A. (1979) *J. Am. Chem. Soc. 101*, 1645–1654.

Oosterhuis, W. T., & Lang, G. (1969) *Phys. Rev. 178*, 439–456.

Osvath, S. R. (1986) *J. Am. Chem. Soc. 108*, 5288–5297.

Peisach, J., Blumberg, W. E., & Wyluda, B. J. (1971) *Proc. Eur. Biophys. Congr.*, 1st, 109–112.

Peisach, J., Mims, W. B., & Davis, J. L. (1979) *J. Biol. Chem. 254*, 12379–12389.

Philips, S. E. V. (1980) *J. Mol. Biol. 142*, 531–554.

Poulos, T. L., Freer, S. T., Alden, R. A., Edwards, S. L., Skogland, U., Takio, K., Eriksson, B., Xuong, N.-h., Yonetani, T., & Kraut, J. (1980) *J. Biol. Chem. 255*, 575–580.

Redhouse, A. D. (1973) *J. Chem. Soc., Dalton Trans. 3*, 1106–1108.

Rhynard, D., Lang, G., Spartalian, K., & Yonetani, T. (1979) *J. Chem. Phys. 71*, 3715–3721.

Rudin, M., Schweiger, A., & Gunthard, Hs. H. (1982) *Mol. Phys. 46*, 1027–1044.

Safo, M. K., Gupta, G. P., Walker, F. A., & Scheidt, W. R. (1991) *J. Am. Chem. Soc. 113*, 5497–5510.

Safo, M. K., Gupta, G. P.; Watson, C. T., Simonis, U., Walker, F. A., & Scheidt, W. R. (1992) *J. Am. Chem. Soc. 114*, 7066–7075.

Satterlee, J. D. (1986) *Annu. Rep. NMR Spectrosc. 17*, 79–178.

Satterlee, J. D., & La Mar, G. N. (1975) *J. Am. Chem. Soc. 98*, 2804–2808.

Scheidt, W. R., & Reed, C. A. (1981) *Chem. Rev. 81*, 543–555.

Scheidt, W. R., Lee, Y. J., Luangdilok, W., Haller, K. J., Anzai, K., & Hatano, K. (1983) *Inorg. Chem. 22*, 1516–1522.

Scholes, C. P., Lapidot, A., Mascarenhas, R., Inubushi, T., Isaacson, R. S., & Feher, G. (1982) *J. Am. Chem. Soc. 104*, 2724–2735.

Scholes, C. P., Falkowski, K., Chen, S., & Bank, J. (1986) *J. Am. Chem. Soc. 108*, 1660–1671.

Schweiger, A. (1982) *Struct. Bonding (Berlin) 51*,

Shulman, R. G., Glarum, S. H., & Karplus, M. (1971) *J. Mol. Biol. 57*, 93–115.

Senn, H., Keller, R. M., & Wüthrich, K. (1980) *Biochem. Biophys. Res. Commun. 92*, 1362.

Soltis, S. M., & Strouse, C. E. (1988) *J. Am. Chem. Soc. 110*, 2824–2829.

Szabo, A., & Perutz, M. (1976) *Biochemistry 15*, 4427–4428.

Takano, T. (1977) *J. Mol. Biol. 110*, 537–568.

Teale, F. W. J. (1959) *Biochim. Biophys. Acta 35*, 543.

Taylor, C. P. S. (1977) *Biochim. Biophys. Acta 491*, 137–149.

Townes, C. H., & Daily, B. P. (1949) *J. Chem. Phys. 17*, 782–796.

Vickery, L., Nozawa, T., & Sauer, K. (1975) *J. Am. Chem. Soc. 98*, 343–350.

Walker, F. A., & Simonis, U. (1991) *J. Am. Chem. Soc. 113*, 8652–8657.

Walker, F. A., Huynh, B. H., Scheidt, W. R., & Osvath, S. R. (1986) *J. Am. Chem. Soc. 108*, 5288–5297.

Wu, J. Z., La Mar, G. N., Yu, L. P., Lee, K. B., Walker, F. A., Chiu, M. L., & Sligar, S. G. (1991) *Biochemistry 30*, 2156–2165.